An Optimization of GlueX FCAL Light Guide Design

C. Cude, R. Mitchell, M. Shepherd, and S. Teige

July 23, 2007

The GlueX detector will use a lead glass electromagnetic calorimeter for reconstructing the energies of photons with polar angle less than 11°. The proposed design consists of 2,800 lead glass elements measuring 4 cm × 4 cm × 45 cm stacked in a roughly circular array, each paired with a 2.4 cm diameter (active area) FEU 84-3 photo-multiplier tube (PMT). The basic design, as well as most of the parts, of the GlueX forward calorimeter are recycled from previous experiments, namely BNL E852 [1] and RadPhi [2]. As incoming photons strike the glass they produce electromagnetic showers. Each shower particle in turn radiates Cherenkov photons as it moves through the glass. The number of such photons detected by the PMTs, and thus the reconstructed energy of the original photon, is proportional to the integrated path length of the shower particles, subject to statistical fluctuations in the development of the shower and propagation and detection of the Cerenkov photons. The resolution of the reconstructed energy is given by:

$$\frac{\sigma_E}{E} = \frac{A}{\sqrt{E}} + B. \tag{1}$$

The floor term, B, is intrinsic to the detector and reconstruction algorithm, and the statistical term, A, accounts for the aforementioned fluctuations but is dominated by photoelectron counting statistics [2]. Thus, increasing the optical efficiency of the system can significantly reduce the portion of the energy resolution of the calorimeter.

As configured in RadPhi each PMT was separated from its lead glass block by an air gap. While an air gap was convenient in terms of detector assembly, maintenance, cost, and mechanical issues, it was the primary limiting factor in light collection, resulting in a statistical term A=7.3% [2]. The inefficiency of the air gap is mostly due to internal reflection (a consequence of the high index of refraction of lead glass and the angular distribution of Cherenkov light) in the glass and the fact that the PMT window covers only a fraction of the back face of each lead glass block. Ideally, a light guide could be used to resolve or diminish both of these problems in the GlueX forward calorimeter. In the following studies we attempt to understand the propagation and collection of light in a single element of the forward calorimeter aiming to design a light guide to improve optical performance and satisfy mechanical requirements and quantify the resulting improvement in resolution.

We begin by developing an analytical calculation of the transmission efficiency from the lead glass to the PMT as a function of the refractive index of the material filling the gap between them. The probability of transmission[1] of light from a medium of index of refraction n_1 into a medium with index of refraction n_2 is given by

$$T(\theta_1) = \begin{cases} 1 - \left[\frac{\sin(\theta_1 - \theta_2)}{\sin(\theta_1 + \theta_2)}\right]^2 & \theta_1 < \theta_C \\ 0 & \theta_1 \geq \theta_C \end{cases} \tag{2}$$

where θ_1 is the initial angle of incidence (in the lead glass) and θ_2 is given by (from Snell's law)

$$\theta_2 = \sin^{-1}\left(\frac{n_1}{n_2}\sin\theta_1\right). \tag{3}$$

[1]This probability depends on the polarization of the incident light, and the expression given here is for the perpendicular case. While Cherenkov radiation tends to produce photons polarized parallel to the plane of incidence we choose to use the equation for perpendicular polarization as a worst case scenario.

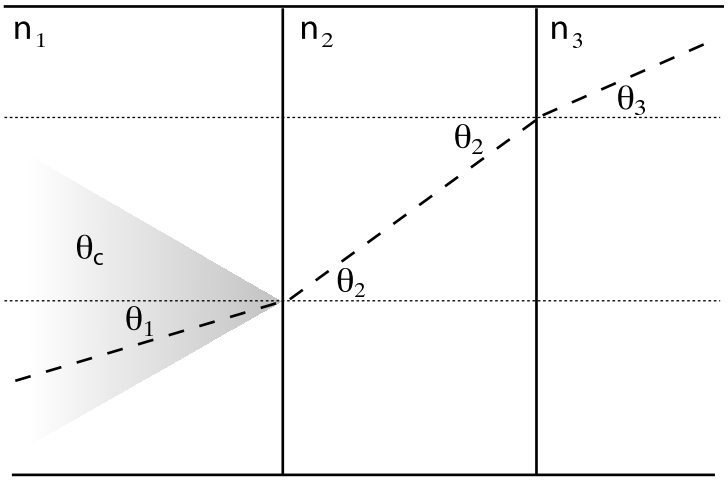

Figure 1: Definition of angles relevant to 2.

For light distributed as

$$\frac{dN}{d\cos\theta} = W(\cos\theta) \tag{4}$$

the fraction transmitted across the interface is

$$\mathcal{F} = \frac{\int W(\theta)T(\theta)d\cos\theta}{\int W(\theta)d\cos(\theta)}. \tag{5}$$

For Cerenkov light generated by an electromagnetic shower in lead glass, $W(\theta)$ can be calculated by Monte-Carlo methods. Figure 2 shows this distribution for showers initiated by 1 GeV photons at various angles of incidence.

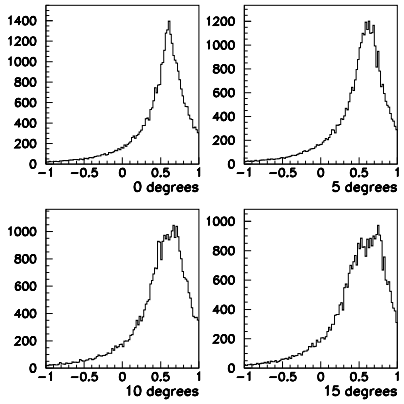

Figure 2: The angular distribution of Cherenkov photons generated by a 1 GeV photon at various angles of incidence. Horizontal axis is the cosine of the angle between the photon and the block axis.

Photons with $\cos\theta > 1/n_1$ will be propagated in a lead glass block by total internal reflection. In this range of angles W for normal incidence, 1 GeV photons (top left of Figure 2) is approximated by

$$W \propto \exp(-4\cos\theta). \tag{6}$$

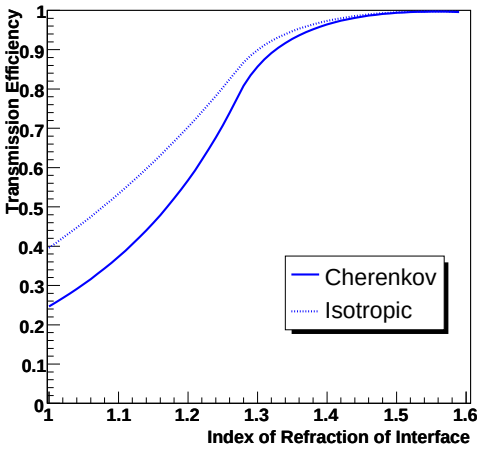

(a) Average transmission efficiency through three media as a function of n_2.

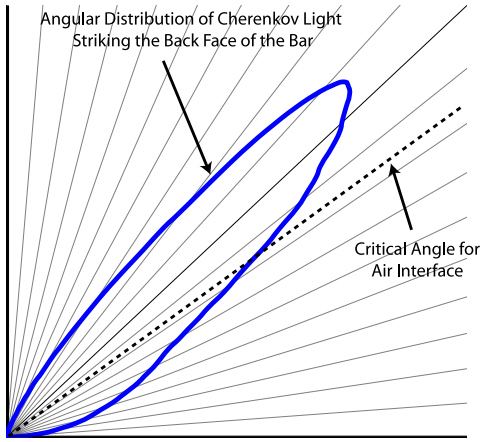

(b) A polar plot of the angular distribution of Cherenkov light striking the back of the block. The dashed line represents the critical angle for internal reflection at the back face and is shown here for transmission into an air gap. Raising n_2 corresponds to rotating the dashed line to the left.

Figure 3: Transmission at the back face.

Assuming that only photons propagated by total internal reflection from the lateral faces of the block reach the back of the lead glass, the critical angle for light reflecting from the sides of the glass (this is also the Cherenkov angle for a shower particle traveling parallel to the axis of the block) determines the maximum angle at which light is incident on the back face of the block and hence the limit of integration in this model. Since the model ignores light at higher angles, it is likely an over estimate of the average transmission efficiency at the back face. Equations 2-6 above were used to calculate, via numerical integration, the average transmission efficiency for a given angular distribution of photons from the lead glass, through an intermediate material, and into the PMT, as a function of the refractive index of the intermediate material. The refractive indices n_1 and n_3 were taken to be 1.62 and 1.5, respectively.

Evaluating the efficiency with $n_2 = 1.0$ (air) gives $\mathcal{F}$=24.7% for perpendicular polarization. As n_2 increases, fewer photons are subject to total internal reflection (TIR) at the back face, and losses due to total internal reflection at the back face eliminated when $n_2 \approx 1.28$. As n_2 continues to increase reflection at the $n_1 - n_2$ interface decreases as given by Equation 2. When n_2 passes 1.58 efficiency begins to drop as reflection at the $n_1 - n_3$ interface increases. The resulting maximum is very slight compared to the gain from eliminating total internal reflection at the back face. Under these conditions, introducing an air gap between the lead glass and PMT reduces the available light by a factor of 0.247 (this is actually an overestimation, because this model ignores light traveling above the critical angle for propagation down the block).

In practice, further losses arise from the fact that the active area of the FEU-84-3 PMT covers roughly 28% of the face of a lead glass block. Thus, an estimate for the efficiency is 28% $\times$ 25%. The latter number can be improved by boosting the coupling material's index of refraction, and the former by increasing the effective aperture of the PMT. This could be achieved with a concentrating light guide. However, designing a concentrator geometry for light at relatively high angles to the central axis is surprisingly difficult (perfect concentration is not possible [3]). Some obvious candidates, e.g. a cone, can actually hamper transmission [4]. More complicated options, like compound parabolic concentrators, are difficult to simulate using the numerical integration methods above. To validate and improve our ability to numerically calculate transmission efficiency and to explore various options for light guide geometries, we have constructed a test setup and a GEANT 4 [5] simulation to verify these calculations and explore various means of coupling the PMTs to the lead glass.

Experimental Setup and Systematic Checks

The bench test was designed to determine the transmission efficiency of the optical joint as a function of incident angle. It consists of a light source, a single 4 cm × 4 cm × 45 cm × type F8 lead glass block, and an FEU-84-3 PMT all contained in a light tight box. An LED continuously produces blue (465 nm) light, which is routed to the box via optical fiber. The optical fiber delivers a forward peaked angular distribution of light. In order to cover a wide range of angles, the fiber can be mounted to the face of the lead glass opposite the PMT or to one of three acrylic prisms mitered at 22.5°, 45°, and 67.5°and fixed to the block with transparent epoxy.

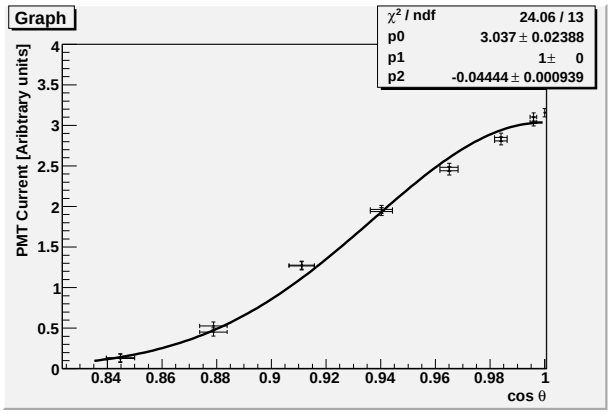

Figure 4: . The angular distribution of light emitted by the fiber was measured by masking the PMT, leaving only a 1 mm^2 aperture. The optical fiber was moved past the PMT transversely and the PMT current was recorded. The distribution is well described by a Gaussian with $\sigma \approx 17°$.

The dynode current was measured by recording the voltage across the bleed down resistor in the PMT base. We measured this voltage for each of the available mounting angles and for both air and optical grease interfaces (Bicron BC-630 with $n \approx 1.465$). The output of the LED was monitored with a photodiode to allow detection of drift in the source intensity and normalization of the PMT current measurements. While our analytical techniques allow us to calculate the absolute transmission efficiency, our experimental setup does not permit such a measurement. Thus, we use the ratio of the voltages (hereafter relative efficiencies) measured for different angles and couplings (the ratio of the numbers of detected photons in the simulations), which are independent of absolute scale, to compare the bench test and simulation data.

Results

The relative efficiencies for various angles are shown in Figure 5. As incident angle increases, relative efficiencies also increase, which is consistent with the expectation that light traveling at steeper angles suffers greater losses to internal reflection at the back face of the block. However, the analytical model developed above fails to reproduce the experimental data. Specifically, the simulation breaks down at higher angles and predicts lower relative efficiencies (cf. data points for 45°in Figure 5) than are observed. The mode of failure suggests that the model does not accurately reproduce the lateral surface interactions, the fine details of which become relevant as higher incident angles lead to more bounces down the bar, as well as that higher angle photons are important. Although these photons are not propagated my TIR, they are not all lost.

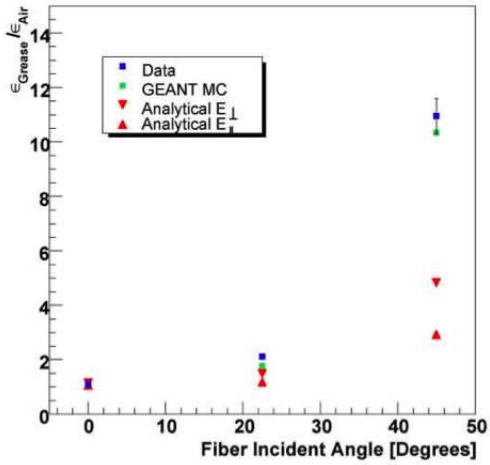

Figure 5: The tuned GEANT model of the block recreated the measurements much more accurately than did the analytical model.

The GEANT Model

We developed a more complete representation of the bench setup in GEANT 4 that incorporates a realistic light source, more detailed geometry, second order corrections to the treatment of optical surfaces and allows ray tracing. The geometry of the GEANT simulation includes the acrylic prisms, optical coupling, PMT window and photocathode. The light source produces optical photons using the measured angular distribution of light from the fiber and can be placed 1 mm away from any of the acrylic prisms or the front face of the block.

Optical processes are simulated in the GEANT simulation under the UNIFIED model [6, 7], which takes into account a number of parameters that describe properties of optical surfaces. The model considers a surface to be composed of smooth micro-facets that can be offset from the plane of the surface. The user defines the distribution of micro-facet offsets (i.e. the severity of surface imperfections) via the parameter σ_α. Other parameters describe the probability that a photon will strike an offset micro-facet at each surface interaction (i.e. what portion of the surface is rough) and the probability that a photon will be reflected back along its original path.

Since the precise surface properties of the lead glass were not known, we developed a procedure to explore the full reasonable parameter space and tuned the parameters so that the behavior of the simulation matched that of the actual lead glass bar used in the bench test. For each of the parameters, we evenly divided a broad range of arbitrarily chosen values and calculated the model output for each combination of the parameter values. To identify the optimal surface parameters, a quantity comparing simulated to measured values was constructed (10) and minimized. Equation 7 gives the ratio of PMT currents (the number of detected photons in the simulation) observed with grease and air couplings for a given fiber mount angle. Equations 8 and 9 give ratios of currents (numbers of photons) observed at consecutive fiber mount angles for grease and air couplings, respectively. Again, the bench test does not provide a measurement of absolute transmission efficiency, so we are forced to use these ratios to compare the data from the simulation and bench test.

$$R_\theta = \frac{PMT_{grease,\theta_i}}{PMT_{air,\theta_i}} \tag{7}$$

$$S_{\theta_i} = \frac{PMT_{grease,\theta_i}}{PMT_{grease,\theta_{i+1}}} \tag{8}$$

$$T_{\theta_i} = \frac{PMT_{air,\theta_i}}{PMT_{air,\theta_{i+1}}} \tag{9}$$

$$X = \left(\frac{R_\theta^{\text{meas.}} - R_\theta^{\text{sim.}}}{\delta_{R_\theta^{\text{meas.}}}}\right)^2 + \left(\frac{S_{\theta_i}^{\text{meas.}} - S_{\theta_i}^{\text{sim.}}}{\delta_{S_{\theta_i}^{\text{meas.}}}}\right)^2 + \left(\frac{T_{\theta_i}^{\text{meas.}} - T_{\theta_i}^{\text{sim.}}}{\delta_{T_{\theta_i}^{\text{meas.}}}}\right)^2 \tag{10}$$

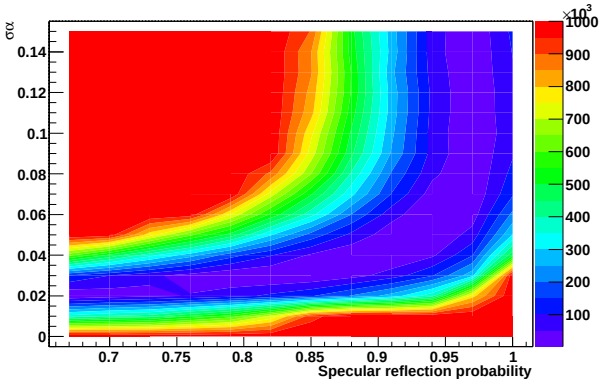

Figure 6: Simulation error as a function of micro-facet offset and percentage of smooth surface area.

Figure 6 shows the value of Eq. 10 as a function of the surface parameters that control the amounts of diffuse and specular reflection in the lead glass. A small amount of diffuse reflection most accurately reproduces the bench data. As expected, this requirement is satisfied on a band of parameter values in Figure 10. The lower left corner of the plot corresponds to many small surface imperfections, and the upper right corresponds to few but comparatively severe imperfections. The optimal set of surface parameters includes an 18% probability of diffuse reflection. This is not unreasonable given that the corners of the bars are coarsely ground. In fact, an air coupled PMT depends on these imperfections. The bulk of Cherenkov radiation produced in the block travels at angles such that it is subject to TIR on both the lateral and terminal faces of the block. Only diffusion resulting from the surface imperfections allows light to escape.

Modeling Light Guides in GEANT

Having obtained the surface properties of the lead glass, we created a second simulation in order to test various light guides under normal operating conditions. The acrylic prisms are removed, and a mirrored light pipe of variable geometry is added between the lead glass and PMT. The light source produces single 1 GeV photons at normal incidence, and the relevant physics processes are added to simulate electromagnetic showers in the lead glass.

Data taken for each Cherenkov photon striking the back face of the block include incident angle and position on the back face of the block at the photon's first and last intersections, whether or not it is reflected back into the bar upon striking the back face, and whether or not it is detected by the PMT[2]. The plots in Figures below present these data for each light guide geometry. For each light guide, the left-most plot is the detection efficiency as a function of the X-Y position of photons striking the back face of the block. The middle plot shows the angular distribution of photons striking the back of the block for the first time and (in tan) the portion of that distribution that is reflected back into the block. The final plot shows the angular distribution for photons exiting the back of the block and (triangles) the detection efficiency as a function of angle of incidence.

Air coupling was simulated with a 2 mm separation between the back face of the block and the PMT window. As expected, most of the light striking the back face for the first time is internally reflected. Surface imperfections cause more diffusion for photons taking multiple trips across the bar, and a comparison of the grey histograms in the middle and right-most plots reveals this effect. The angular photon collection

[2]During the development of the photon tracking code, it became apparent that in the simulation a few shower particles occasionally survived to exit the back of the lead glass block.

efficiency has a sharp cutoff at the critical angle for transmission into air and approaches the geometric factor at more forward angles. The collection efficiency for photons traveling at steeper angles is very slightly higher because they may reach the PMT from a larger portion of the back face than photons at more forward angles. The angular efficiency is not quite zero for photons outside the TIR angle as a consequence of the slight roughness of the block.

The simplest light guide design tested was a right cylindrical piece of acrylic with the same diameter as the active area of the PMT and 5 centimeters in length (this length is derived from the working estimate for the setback needed to satisfy magnetic shielding requirements [8]). Such a light guide would only serve to eliminate internal reflection at the back face of the block and efficiently convey photons to the PMT. The bulk of light reaching the back face of the block travels at near the critical angle for propagation down the block, so TIR will not propagate light effectively in an acrylic cylinder. Hence, mirrored and unmirrored versions of the light pipe were tested.

Mirror coating the light pipe allows near uniform detection efficiency across the face of the light pipe and prevents photons from entering the sides. Reflection within the lead glass is substantially reduced as compared to an air gap. Detection efficiency for photons entering the light pipe is very high, so the average detection efficiency for all photons striking the back of the block approaches the geometric limit of roughly 25%. The enhancement near $\cos\theta = 0.75$ is a result of light trapped within the lead glass getting multiple chances to enter the light guide as it travels up and down the bar. Photons entering the unmirrored light pipe near the edges are more likely to make it to the PMT with fewer bounces than those entering near the center, hence the enhancement around the edges. Note that a few photons enter the sides of the light pipe and are detected. High angle photons leak from the sides of the light pipe suppressing detection efficiency until TIR is in effect at more forward angles, but the same boost in efficiency due to trapping is observed as in the mirrored case.

One candidate for a concentrating light guide used a conical geometry. In order to eliminate internal reflection across the entire back face and minimize the geometric mismatch, the base of the cone has a radius just large enough to reach the corners of the lead glass bar. The portions of the cone extending beyond the lead glass are then removed leaving a shape reminiscent of the sharpened end of a pencil.

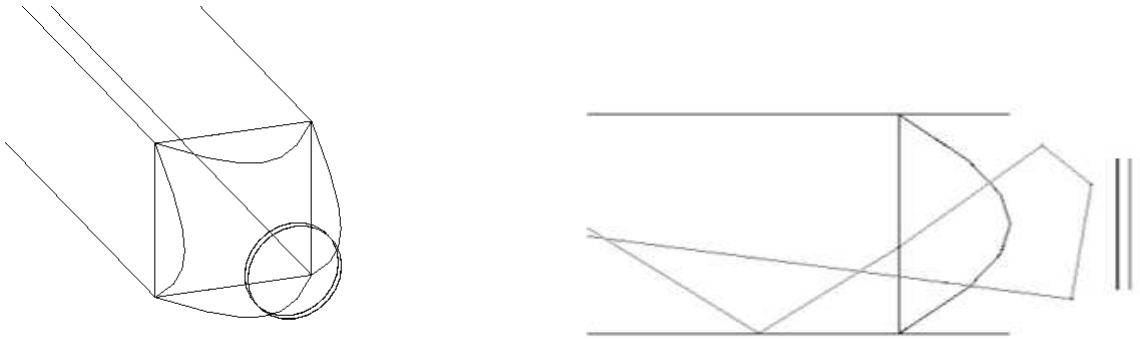

(a) Light guide mounted on a lead glass block with the optical interface and PMT window at the narrow end.

(b) A photon entering the light guide, reflecting from the sides, and returning to the lead glass.

Figure 7: The pencil-type light guide.

While intuitive and apparently reasonable at first glance, the conical concentrator is a surprisingly poor performer. The sloping sides of a conical acrylic light guide make mirroring critical, but even when leakage is eliminated the conical light guide is less efficient than the light pipe. This is primarily due to the fact that photons making several reflections against the sides of the light guide before reaching the PMT are likely to be sent back into the lead glass. Each time a photon reflects off of the sloping sides its path is deflected away from the PMT. Given sufficiently high initial angle or enough bounces, photons are actually sent back into the lead glass. Decreasing the slope of the sides so that the light guide is a simple frustum of

Table 1: The performance of various light guide geometries. The air gap geometry, used in RadPhi, is taken as the baseline. In RadPhi the statistical term on the photon energy resolution was 7.3%. It was further estimated that photon counting statistics were a 6.0% contribution to that resolution.

	Efficiency	Photon Counting Error	Statistical Term
Air Gap	9.0%	6.0%	7.3%
Pencil	17.2%	4.3%	6.0%
Cone	18.0%	4.2%	5.9%
Unmirrored Pipe	22.0%	3.8%	5.6%
Mirrored Pipe	27.4%	3.4%	5.4%
Winston Cone	27.6%	3.4%	5.3%

Table 2: The performance of mirrored light pipes with lengths between one and eight centimeters.

	1 cm	2 cm	3 cm	4 cm	5 cm	6 cm	7 cm	8cm
Collection Efficiency	28.2%	28.2%	28.2%	27.9%	27.4%	27.0%	26.5%	26.2%

a cone (see the "narrow cone" below) increases the efficiency, but not to the level of the light pipe.

Typically the best concentrator design is the compound parabolic concentrator [4] (otherwise known as the Winston cone). Winston cones (assuming perfect reflectivity) have a geometrically determined acceptance angle within which efficiency is very nearly 100% and beyond which very nearly zero. Unfortunately, there is little if any literature describing the use of Winston cones to concentrate light through a step down in refractive index. Furthermore, the geometry of the Winston cone is somewhat complicated and thus difficult to simulate in GEANT directly. Instead, we used a separate Fortran routine called Wico, which determines the shape of the Winston cone based only on user specified entrance and exit apertures. It is therefore not certain that the Winston cone simulated here is optimal.

The average photon collection efficiency for various light guides is given in Table 1. The light guide used in the GlueX FCAL must be cost effective, facilitate magnetic shielding of the PMTs and allow disassembly and maintenance of the detector. While the Winston cone provides the greatest potential enhancement it is complicated to manufacture and does not reach its peak performance with cost effective materials. A mirrored acrylic light pipe sacrifices little performance compared to the acrylic Winston cone and is comparatively simple to produce.

While mechanical and magnetic shielding requirements prohibit an ideal (i.e. very short) light pipe, the length of the light pipe can be adjusted without seriously affecting performance. The length requirements for the light guide derive from the need to recess the PMTs several centimeters into magnetic shielding to allow them to operate in the fringe field of the solenoid [8]. Imperfect mirroring and bulk absorption causes some light loss in longer light pipes; the dependence of light pipe performance on length is given in Table 2. Minimizing the length, and thus the average number of reflections necessary for a photon to traverse the light pipe, and maximizing the reflectivity of the light pipe should be production priorities.

Among the available options, the light pipe most fully satisfies the requirements for the the GlueX FCAL, while still allowing for the adjustments and adaptations necessary to fit the mechanical and material limitations. Including a well made acrylic light pipe in the GlueX forward calorimeter may, for modest cost, improve light collection by more than a factor of three, and thus reduce the statistical term of the energy resolution by 25%-30%.

References

[1] R. R. Crittenden, *et al.* A 3000 element lead-glass electromagnetic calorimeter. *Nuclear Instruments and Methods in Physics Research A*, 387:377–394, 1997.

[2] R.T. Jones, *et al.* Performance of the radphi detector and trigger in a high rate tagged photon beam. *Nuclear Instruments and Methods in Physics Research A*, 570:384–398, 2007.

[3] Albert Arakengy. Liouville's theorem and the intensity of beams. *American Journal of Physics*, 25(8):519–525, November 1957.

[4] W.T. Welford and R. Winston. *High Collection Nonimaging Optics*. Academic Press, 1989.

[5] S. Agostinelli, *et al.* Geant4-a simulation toolkit. *Nuclear Instruments and Methods in Physics Research A*, 506(3):250–303, July 2003.

[6] A. Levin, *et al.* A more physical approach to model the surface treatment of scintillation counters and its implementation into detect. November 1996.

[7] C. Moisan, *et al.* Towards a model accounting for the impact of surface treatment on the performances of scintillation counters. 1997.

[8] S. Denisov, *et al.* Studies of magnetic shielding for phototubes. *Nuclear Instruments and Methods in Physics Research A*, 533:467–474, 2004.

Figures

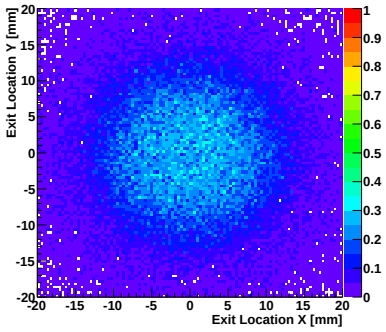

(a) Detection efficiency as a function of position.

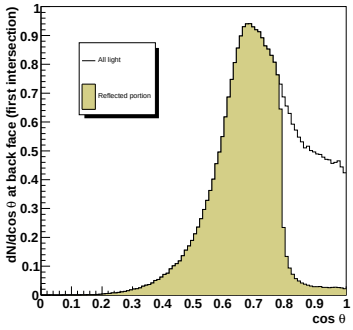

(b) Angular photon distribution (first strike) and reflected portion.

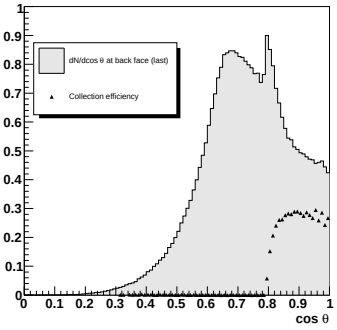

(c) Angular photon distribution (last strike) and detection efficiency.

Figure 8: Performance characteristics of an air gap.

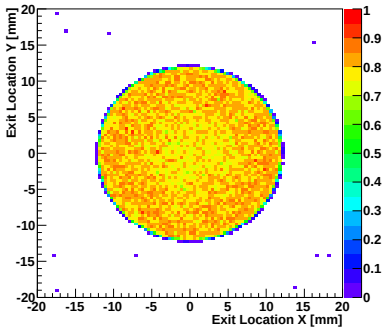

(a) Detection efficiency as a function of position.

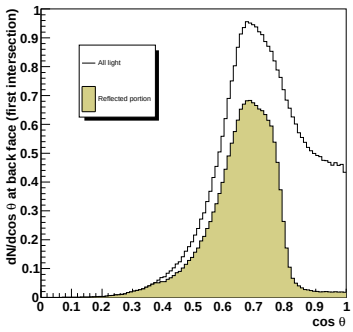

(b) Angular photon distribution (first strike) and reflected portion.

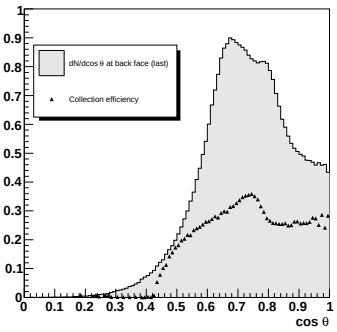

(c) Angular photon distribution (last strike) and detection efficiency.

Figure 9: Performance characteristics of a mirrored light pipe.

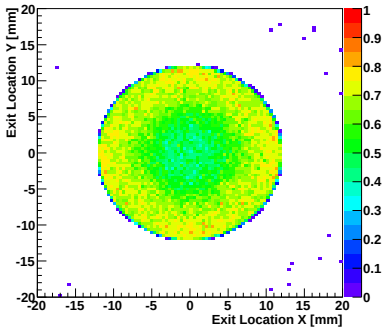

(a) Detection efficiency as a function of position.

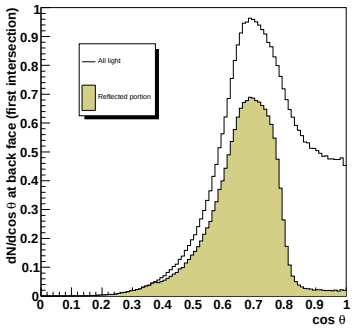

(b) Angular photon distribution (first strike) and reflected portion.

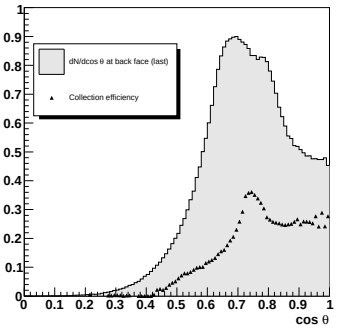

(c) Angular photon distribution (last strike) and detection efficiency.

Figure 10: Performance characteristics of an unmirrored light pipe.

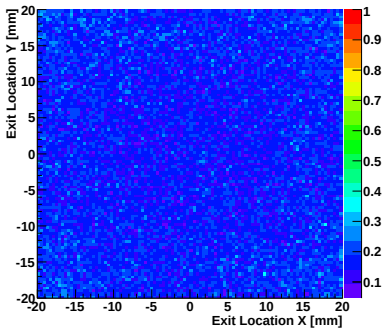

(a) Detection efficiency as a function of position.

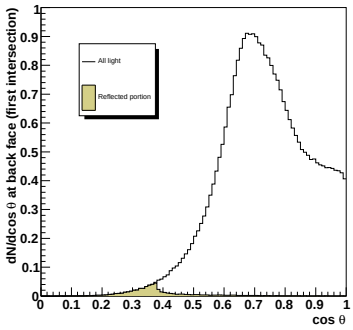

(b) Angular photon distribution (first strike) and reflected portion.

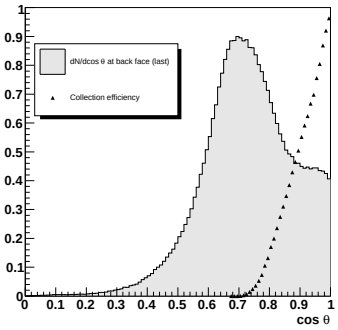

(c) Angular photon distribution (last strike) and detection efficiency.

Figure 11: Performance characteristics of a mirrored pencil-type light guide.

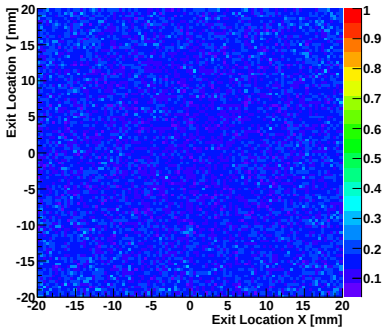

(a) Detection efficiency as a function of position.

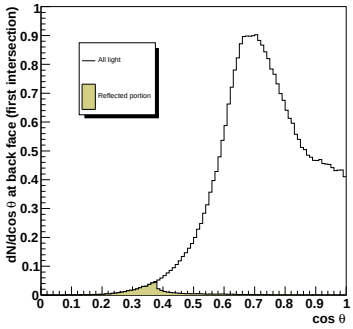

(b) Angular photon distribution (first strike) and reflected portion.

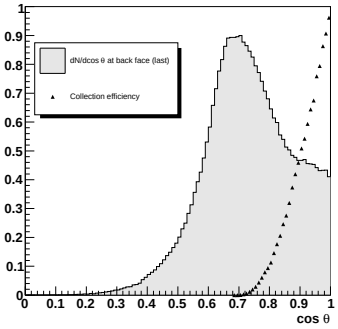

(c) Angular photon distribution (last strike) and detection efficiency.

Figure 12: Performance characteristics of an unmirrored pencil-type light guide.

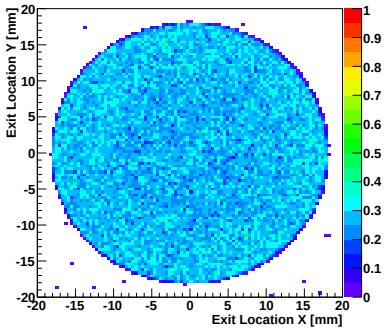

(a) Detection efficiency as a function of position.

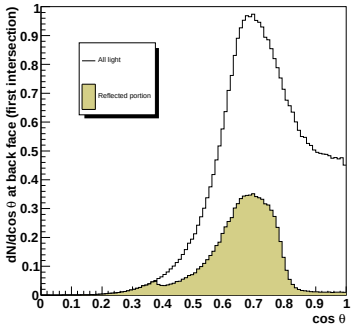

(b) Angular photon distribution (first strike) and reflected portion.

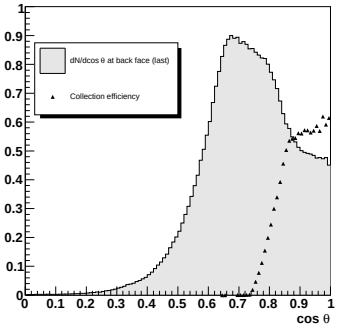

(c) Angular photon distribution (last strike) and detection efficiency.

Figure 13: Performance characteristics of a mirrored narrow conical light guide.

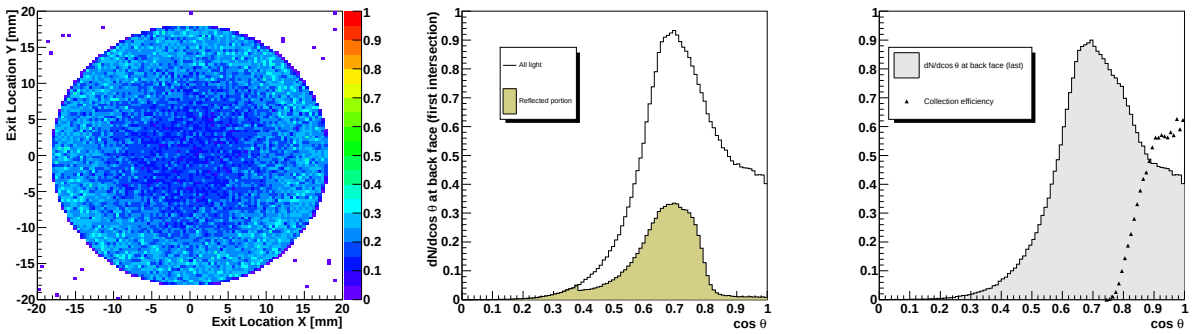

(a) Detection efficiency as a function of position.

(b) Angular photon distribution (first strike) and reflected portion.

(c) Angular photon distribution (last strike) and detection efficiency.

Figure 14: Performance characteristics of an unmirrored narrow conical light guide.

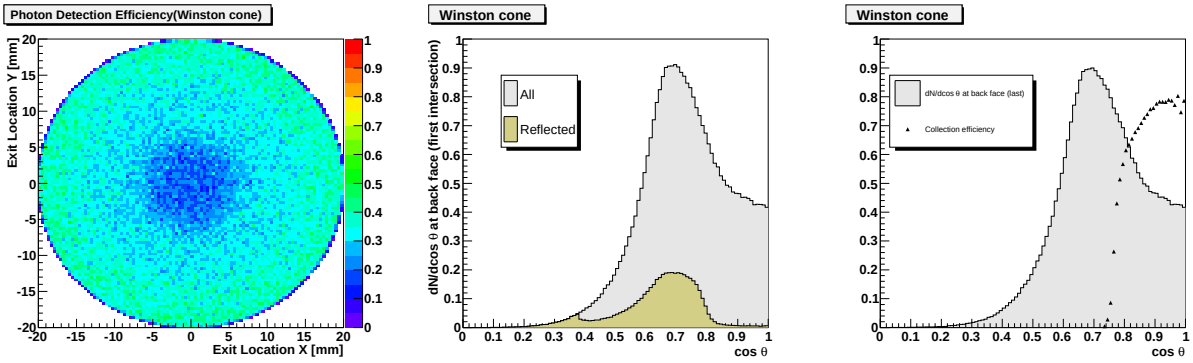

(a) Detection efficiency as a function of position.

(b) Angular photon distribution (first strike) and reflected portion.

(c) Angular photon distribution (last strike) and detection efficiency.

Figure 15: Performance characteristics of a Winston cone.